Global Biogeochemical Cycles

RESEARCH ARTICLE
10.1029/2023GB007919

Early Diagenetic Controls on Sedimentary Iodine Release and Iodine-To-Organic Carbon Ratios in the Paleo-Record

Florian Scholz[1,2], Dalton S. Hardisty[3], and Andrew W. Dale[1]

[1]GEOMAR Helmholtz Centre for Ocean Research Kiel, Kiel, Germany, [2]Now at Institute for Geology, Center for Earth System Research and Sustainability, Universität Hamburg, Hamburg, Germany, [3]Department of Earth and Environmental Sciences, Michigan State University, East Lansing, MI, USA

Key Points:

- The impact of early diagenesis on benthic iodine fluxes and iodine burial was quantitatively evaluated using a reaction-transport model
- Dissolved iodine anomalies in the water column are indicative of benthic efflux from anoxic sediments with high organic carbon turnover
- Not only bottom water oxygen but also organic carbon delivery and sedimentation rate determine sedimentary iodine-to-organic carbon ratios

Supporting Information:

Supporting Information may be found in the online version of this article.

Correspondence to:

F. Scholz,
florian.scholz@uni-hamburg.de

Citation:

Scholz, F., Hardisty, D. S., & Dale, A. W. (2024). Early diagenetic controls on sedimentary iodine release and iodine-to-organic carbon ratios in the paleo-record. *Global Biogeochemical Cycles*, *38*, e2023GB007919. https://doi.org/10.1029/2023GB007919

Received 19 JUL 2023
Accepted 20 JAN 2024

Author Contributions:

Conceptualization: Florian Scholz, Dalton S. Hardisty, Andrew W. Dale
Formal analysis: Florian Scholz, Andrew W. Dale
Funding acquisition: Florian Scholz, Dalton S. Hardisty, Andrew W. Dale
Investigation: Florian Scholz, Dalton S. Hardisty
Methodology: Florian Scholz, Dalton S. Hardisty, Andrew W. Dale
Resources: Florian Scholz
Validation: Florian Scholz
Writing – original draft: Florian Scholz

Abstract Iodine cycling in the ocean is closely linked to productivity, organic carbon export, and oxygenation. However, iodine sources and sinks at the seafloor are poorly constrained, which limits the applicability of iodine as a biogeochemical tracer. We present pore water and solid phase iodine data for sediment cores from the Peruvian continental margin, which cover a range of bottom water oxygen concentrations, organic carbon rain rates and sedimentation rates. By applying a numerical reaction-transport model, we evaluate how these parameters determine benthic iodine fluxes and sedimentary iodine-to-organic carbon ratios ($I:C_{org}$) in the paleo-record. Iodine is delivered to the sediment with organic material and released into the pore water as iodide (I^-) during early diagenesis. Under anoxic conditions in the bottom water, most of the iodine delivered is recycled, which can explain the presence of excess dissolved iodine in near-shore anoxic seawater. According to our model, the benthic I^- efflux in anoxic areas is mainly determined by the organic carbon rain rate. Under oxic conditions, pore water dissolved I^- is oxidized and precipitated at the sediment surface. Much of the precipitated iodine re-dissolves during early diagenesis and only a fraction is buried. Particulate iodine burial efficiency and $I:C_{org}$ burial ratios do increase with bottom water oxygen. However, multiple combinations of bottom water oxygen, organic carbon rain rate and sedimentation rate can lead to identical $I:C_{org}$, which limits the utility of $I:C_{org}$ as a quantitative oxygenation proxy. Our findings may help to better constrain the ocean's iodine mass balance, both today and in the geological past.

1. Introduction

Due to its biophilic and redox-sensitive behavior in marine systems, iodine can potentially be used as a (paleo) biogeochemical tracer. Under oxic conditions, iodate (IO_3^-) is the stable form of iodine in seawater. Analogous to the major nutrients nitrate and phosphorus, dissolved iodine is slightly deleted in surface waters indicating that it is taken up by phytoplankton (Wong, 1977; Wong & Brewer, 1974). Unlike the major nutrients, however, iodine concentrations vary within a relatively narrow range around the global average concentration in seawater of 470 nM. Fresh phytoplankton is characterized by a molar iodine-to-carbon ratio (I:C) of around $1.4 \pm 0.8 \times 10^{-4}$ (Elderfield & Truesdale, 1980) corresponding to an iodine-to-nitrogen ratio (I:N) of $9.3 \pm 5.3 \times 10^{-4}$ assuming a Redfield-like carbon-to-nitrogen ratio of 106:16. Under mildly reducing conditions, IO_3^- is reduced to iodide (I^-). The redox potential of the half reaction is in between the oxygen-H_2O and nitrate-nitrite redox couples, meaning that IO_3^- reduction takes place in oxygen-depleted water masses (Cutter et al., 2018; Wong & Brewer, 1977). Conversely, I^- oxidation requires oxygen (O_2) and cannot proceed under nitrogenous, manganous or ferruginous conditions (Cutter et al., 2018; Luther, 2023). Accordingly, I^- enrichment at the expense of IO_3^- is observed in the oxygen minimum zones (OMZs) of the northeastern and southeastern equatorial Pacific and the Arabian Sea (Cutter et al., 2018; Farrenkopf et al., 1997; Moriyasu et al., 2020; Rapp et al., 2020; Rue et al., 1997), where oxygen concentrations drop to very low values (<2 μM). The reduction of IO_3^- to I^- under oxygen-deficient conditions forms the basis for the use of iodine-to-calcium ratios in marine carbonates as a paleo-redox proxy. Marine calcifying organisms incorporate IO_3^- in their shells replacing carbonate, whereas I^- is incompatible (Feng & Redfern, 2018; Lu et al., 2010; Podder et al., 2017). Therefore, low iodine-to-calcium in ancient carbonate shells is interpreted as an indication for reduced IO_3^- concentrations in seawater under oxygen-deficient conditions (Lu et al., 2010).

In the open ocean, the sum of IO_3^- and I^- generally equals the near-conservative concentration of iodine in the ocean (Moriyasu et al., 2023). Closer to the ocean boundaries, however, the sum of IO_3^- and I^- may exceed this concentration. The presence of excess dissolved iodine in the water column has been attributed to I^- release from

Writing – review & editing: Florian Scholz, Dalton S. Hardisty, Andrew W. Dale

anoxic sediments where the OMZ impinges on the seafloor (Cutter et al., 2018; Farrenkopf & Luther, 2002; Moriyasu et al., 2020; Shaikh et al., 2023). Due to its biophilic behavior in the water column, organic matter represents the main source of iodine in marine sediments (Price & Calvert, 1973). During organic matter degradation in surface sediments, iodine is released into the pore water as I^- along with dissolved inorganic carbon (DIC) and nitrogen (as ammonium, NH_4^+) (Kennedy & Elderfield, 1987b; Upstill-Goddard & Elderfield, 1988). In the absence of oxygen in the surface sediment and bottom water, I^- can leak out of the sediment, which can explain the presence of excess dissolved iodine in the water column of OMZs. By contrast, under oxic conditions in the surface sediment, I^- (valence state of −I) is oxidized to diatomic iodine (I_2, valence state of 0), hypoiodous acid (HOI, valence state of +I) and eventually IO_3^- (valance state of +V) (see Luther (2023) for a recent review of the underlying thermodynamics).

While IO_3^- production has been demonstrated in sediments (Kennedy & Elderfield, 1987a, 1987b), the intermediates I_2 and HOI are important precursors (Luther, 2023). These precursors are short-lived but can both form bonds to fresh organic material, thus removing iodine from solution (Francois, 1987; Harvey, 1980; Kennedy & Elderfield, 1987b; Truesdale & Luther, 1995). Under oxic bottom water conditions, these reactions enrich the particulate I:C of surface sediments relative to the I:C of phytoplankton. For this reason, it has been argued that sedimentary iodine-to-organic carbon ratios ($I:C_{org}$) generally increase with bottom water oxygen concentration (BWO_2), which forms the basis for the use of sedimentary $I:C_{org}$ as a paleo-redox proxy (Calvert & Pedersen, 1993; Zhou et al., 2017). However, deeper in the sediment column, at least some excess sedimentary iodine is re-released into the pore waters during ongoing anaerobic organic matter degradation. The corresponding pore waters show elevated I^- to DIC and NH_4^+ ratios compared to the I:C and I:N of phytoplankton (Kennedy & Elderfield, 1987b; Martin et al., 1993; Price & Calvert, 1973, 1977). Ultimately, it remains unclear to what degree, if any, excess sedimentary $I:C_{org}$ observed under oxic bottom waters is retained and preserved in the geologic record.

According to the marine biogeochemistry of iodine outlined above, benthic iodine fluxes and sedimentary $I:C_{org}$ are controlled by the rain rate of organic material to the seafloor (delivering biogenic iodine), the rate of organic matter degradation in the sediment (releasing I^- to the pore water and consuming oxygen) and BWO_2 (controlling the extent of I^- oxidation and formation of excess iodine). Furthermore, the overall sedimentation rate determines the time frame that sediment particles reside at the surface and participate in iodine dissolution and re-precipitation and, thus, the extent to which iodine may be lost to the bottom water or become enriched relative to carbon and nitrogen prior to burial (Kennedy & Elderfield, 1987b). Even though these general factors have been identified decades ago (e.g., Kennedy & Elderfield, 1987a, 1987b; Pedersen & Price, 1980; Ullman & Aller, 1980, 1983, 1985; Upstill-Goddard & Elderfield, 1988), it is still not known how each of these parameters or combinations thereof determine benthic I^- fluxes and $I:C_{org}$ paleo-signals in various seafloor environments.

In an attempt to quantify the effect of each of these factors, we present pore water I^- and solid phase iodine concentration data for sediment cores from two latitudinal transects across the Peruvian continental margin. Our sampling sites cover a range of organic matter rain rates to the seafloor, organic carbon degradation rates and sediment burial fluxes and BWO_2. We apply a numerical reaction-transport model to reproduce the observed iodine distribution in the pore water and sediment and to examine the mechanistic and quantitative constraints on benthic I^- fluxes and $I:C_{org}$. Importantly, the Peruvian margin is also the area of two previous water column iodine speciation surveys (Cutter et al., 2018; Rapp et al., 2020), and an Ocean Drilling Program (ODP) transect (Martin et al., 1993). Our study of shallow sediments thus links these environments and allows for the opportunity to evaluate iodine cycling from the water column to early diagenesis and deep burial.

2. Material and Methods

2.1. Study Area and Samples

The Peruvian margin is an illustrative example for biogeochemical cycling in an open-marine OMZ (Scholz, 2018). Upwelling of nutrient-rich and oxygen-depleted intermediate water along the Peruvian coast causes high rates of primary production (up to 300 mmol carbon m^{-2} d^{-1}) (Pennington et al., 2006). Due to the lateral supply of oxygen-poor water and intense microbial respiration in the subsurface, oxygen concentrations are essentially zero between 100 and 300 m water depth throughout most of the year (Thamdrup et al., 2012). The upper boundary of the Peruvian OMZ is subject to considerable fluctuations related to the passage of coastal-trapped waves, which occur most frequently under El Niño conditions (Gutiérrez et al., 2008; Levin et al., 2002). As a result, oxygen

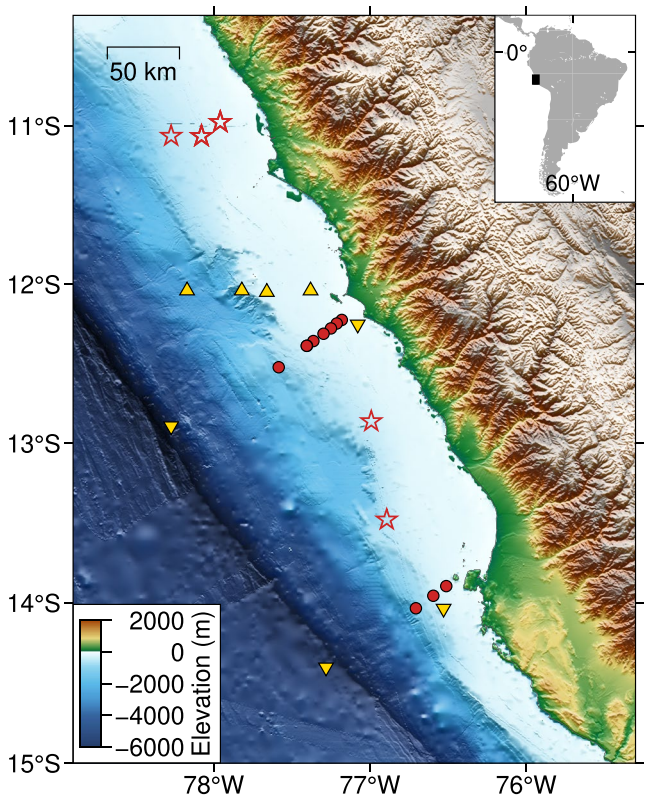

Figure 1. Bathymetric map of the Peruvian continental margin showing the location of MUC sites (red dots). Red stars depict drilling sites of Ocean Drilling Program Leg 112. Upward and downward facing triangles depict water column stations sampled on GEOTRACES cruise GP16 (Cutter et al., 2018) and RV Sonne cruise SO243 (Rapp et al., 2020), respectively.

concentrations on the shallow shelf may vary from 0 to 100 μM within days to weeks (Lüdke et al., 2020). The location of the lower boundary of the OMZ on the upper continental slope is more stable at roughly 400–500 m water depth.

Organic carbon degradation in the anoxic water column is coupled to denitrification (Dalsgaard et al., 2012; Lam et al., 2009), whereas in the underlying sediments sulfate reduction is the dominant organic carbon degradation pathway (Bohlen et al., 2011). Nitrogenous conditions in the water column, as indicated by the presence of a secondary nitrite maximum, are accompanied by elevated concentrations of I^- (Cutter et al., 2018; Rapp et al., 2020). Surface sediments underneath the anoxic water column are mostly ferruginous (presence of Fe^{2+}) and occasionally sulfidic (Plass et al., 2020; Scholz et al., 2011, 2016). Due to the absence of oxygen in the bottom water, pore water dissolved Fe (Fe^{2+}) may leak out of the sediment (Noffke et al., 2012) and plumes of high dissolved Fe concentrations have been observed in the water column (Hong & Kester, 1986; Schlosser et al., 2018; Scholz et al., 2016; Vedamati et al., 2014). Water column Fe anomalies are accompanied by the presence of excess dissolved iodine suggesting that anoxic shelf sediments represent a source of I^- to the water column (Cutter et al., 2018). Lower benthic Fe fluxes as well as iron and excess dissolved iodine concentrations in the water column have been observed after a period of shelf oxygenation (Noffke et al., 2012; Rapp et al., 2020).

Drill cores from OPD Leg 112 revealed highly elevated pore water I^- concentrations in subsurface sediments of the Peruvian continental margin (Martin et al., 1993). Both sedimentary I:C and pore water I^- to NH_4^+ ratios were found to increase from the shelf to slope sites and with increasing BWO_2, which is consistent with the benthic biogeochemistry of iodine outlined above. However, to date, there are no solid phase or pore water iodine data for shallow sediment cores from the Peruvian margin, which could be used to constrain the controls on benthic iodine release and sedimentary iodine enrichment relative to carbon or nitrogen. The longitudinal transects at ∼12° and ∼14°S sampled for this study cover the highly productive shallow shelf with fluctuating oxygen concentrations, the generally anoxic OMZ on the outer shelf and upper slope as well as the area with oxic bottom water below the OMZ (Figures 1 and 2).

2.2. Sampling and Chemical Analyses

Water and sediment samples were collected on RV Meteor cruises M136 and M137 in April and May 2017 (Table 1). Water column samples for oxygen measurements by Winkler titration were collected using a rosette equipped with a CTD sensor. Sediment cores with an undisturbed sediment-water interface (SWI) were retrieved using a multiple corer (MUC). Upon recovery, MUC liners were transferred to an argon-filled glove bag within a cooled laboratory. Prior to incubation, the bottom water was siphoned with a tube and subsequently treated as described below for pore waters. Sediment cores were sectioned at high resolution (1 cm intervals) in the uppermost 6 cm and at gradually increasing resolution at greater depth (2 cm intervals up to 14 cm, then 4 cm intervals). Subsamples for pore water recovery were transferred to centrifuge vials. Another sediment aliquot was transferred to pre-weighed plastic cups for the determination of water content and porosity. The pore water separation was done at seafloor temperature by centrifuging at 4,000 rpm for 20 min. Centrifuge vials were then transferred to another argon-filled glove bag and the pore water was filtered through 0.2 μm cellulose acetate syringe filters. Leftover sediments in centrifuge vials or plastic cups were refrigerated for later solid phase analyses.

Alkalinity was determined shortly after pore water recovery by titration with 0.02 M hydrochloric acid. Pore water concentrations of NH_4^+ and total hydrogen sulfide ($\Sigma H_2S = H_2S + HS^- + S^{2-}$, hereafter referred to as H_2S) were also determined onboard by photometry (see Dale et al. (2016) for details). Pore water samples for I^- analyses were kept frozen until analysis at GEOMAR by ion chromatography with a precision <5% relative standard deviation for replicate analyses.

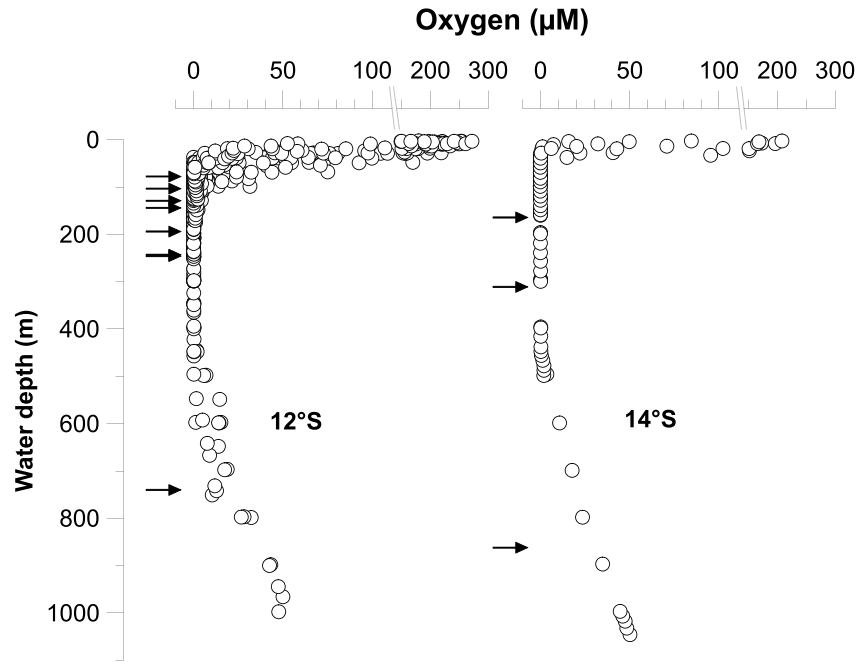

Figure 2. Water column oxygen concentrations measured above the shelf and upper slope (<1,000 m) at (a) 12°S and (b) 14°S. Horizontal arrows depict the water depth of MUC stations on each transect.

Sedimentary organic iodine was determined at Michigan State University using a method adapted from Zhou et al. (2017) and Romarís-Hortas et al. (2009). Specifically, 10–20 mg of sediment were rinsed with 0.5 mL 3% (v:v) nitric acid, sonicated for 1 hr, centrifuged, and the supernatant removed. This step dissolves carbonate-bound iodine. While the dissolution removes carbonate-bound iodine, we note that carbonate-bound iodine is unlikely to contribute to variations in I:C. Specifically, the I:Ca of foraminiferal calcite from the Peruvian margin are reported as extremely low (<2.3 μmol mol^{-1}) due to the low bottom water oxygen conditions (Glock et al., 2014). Even if the Peruvian margin sediment was 100% carbonate, this would equate to <2.9 μg g^{-1} iodine, or <10% of the lowest organic iodine concentration measured in this study. To remove any leftover 3% nitric acid, the samples

Table 1
Sampling Stations

Cruise	Station	Gear	Latitude	Longitude	Water depth (m)	Bottom water oxygen[a] (μM)
12°S transect						
M136	483	MUC8	12°13.52′S	77°10.79′W	78	4.6
M137	787	MUC33	12°14.80′S	77°12.70′W	103	13.9
M136	426	MUC6	12°16.68′S	77°14.95′W	129	Below LOD
M137	651	MUC8	12°18.71′S	77°17.80′W	144	Below LOD
M137	692	MUC15	12°21.50′S	77°21.70′W	194	Below LOD
M136	412	MUC5	12°23.30′S	77°24.18′W	243	Below LOD
M137	595	MUC1	12°23.29′S	77°24.27′W	246	Below LOD
M136	543	MUC9	12°31.35′S	77°35.01′W	740	16.0
14°S transect						
M136	338	MUC1	13°53.69′S	76°30.65′W	164	Below LOD
M136	342	MUC2	13°57.36′S	76°35.63′W	311	Below LOD
M136	409	MUC4	14°02.02′S	76°42.30′W	862	33.1

Note. LOD: Limit of detection of the Winkler method (2–3 μM).
[a]Measured on water samples collected a few meters above the seafloor.

were subsequently rinsed with 1 mL deionized water, sonicated for 1 hr, centrifuged, and the supernatant removed (repeated 5 times). Note that this step could remove inorganic salts as well, but that these have minor iodine (Harvey, 1980). We then added 3–5 mL of 25% tetramethylammonium hydroxide (TMAH) (v:v) for the subsequent organic iodine extractions. For all samples we applied an adapted microwave-assisted extraction (MAE) method already used for organic iodine from seaweed (Romarís-Hortas et al., 2009). We utilized an Anton-Paar Microwave Pro in vented Teflon vials to heat samples to 110°C, with a ramp up time of 10 min and hold time of 5 min. To our knowledge, there are no certified reference materials for sedimentary organic iodine. Thus, to validate our results we additionally measured two sediment samples from the Baltic Sea with I:C_{org} previously determined in Zhou et al. (2017) and 25 of our Peruvian margin samples using a hot plate extraction. For the hot plate extraction, the samples were kept on a hot plate at 90°C for 21 days, with daily sonication for 1 hr. For both extraction techniques, total iodine was quantified in the supernatant (diluted to 1% TMAH) using a ThermoFisher iCAP triple quadrupole ICP-MS. I:C_{org} ratios of the Baltic Sea showed good agreement with those published in Zhou et al. (2017) and the Peruvian margin samples agreed well with the results from the MAE method (see Figures S1 and S2 in Supporting Information S1 for comparison and additional details).

Total organic carbon (C_{org}) and nitrogen (N, presumed equivalent to organic N) in freeze-dried and ground sediment samples were measured using an element analyzer (Euro EA, HEKAtech). Inorganic carbon was removed prior to analyses by treating sediments with 0.25 M hydrochloric acid until the degassing of CO_2 had ceased.

2.3. Reaction-Transport Modeling

2.3.1. Generalized Framework

A 1-D reaction-transport model was set up to simulate carbon, nitrogen and iodine turnover in the upper 50 cm of sediment on the Peruvian shelf, OMZ and below OMZ. It is based on a previous version for simulating carbon and nitrogen turnover in Peruvian sediments (Bohlen et al., 2011; Dale et al., 2016) and expanded here to include a simple iodine cycle. The model considers molecular diffusion, bioturbation, sediment burial and compaction, bioirrigation and biogeochemical reactions. The turnover of solids (S) and dissolved pore fluid species (P) was simulated by applying the following mass balance equations:

$$d_S \cdot (1-\Phi) \cdot \frac{\partial S}{\partial t} = \frac{\partial}{\partial x}\left(d_S \cdot (1-\Phi) \cdot \left(D_B \cdot \frac{\partial S}{\partial t} - w \cdot S\right)\right) + d_S \cdot (1-\Phi) \cdot R_S \quad (1)$$

$$\Phi \cdot \frac{\partial P}{\partial t} = \frac{\partial}{\partial x}\left(\Phi \cdot \left(D_S \cdot \frac{\partial P}{\partial t} - v \cdot P\right)\right) + \Phi \cdot \alpha \cdot (P_{BW} - P) + \Phi \cdot R_S \quad (2)$$

where S is the concentration of solid species in g g^{-1} of dry sediment, P is the concentration of dissolved species in pore fluids in mmol L^{-1}, t is time (yr), x is sediment depth (cm), d_S is the density of dry solids (g cm^{-3}), Φ is sediment porosity, D_B is the bioturbation coefficient (cm^2 yr^{-1}), w is the burial velocity of solids (cm yr^{-1}), R_S is the turnover rates of solid species (g g^{-1} yr^{-1}), R_D is the turnover rate of dissolved species (mmol L^{-1} yr^{-1}), D_S is the molecular diffusion coefficient of solutes in pore water (cm^2 yr^{-1}), v is the burial velocity of pore fluid (cm yr^{-1}), α is the bioirrigation coefficient (yr^{-1}), and P_{BW} is the bottom water concentration of P. The model was set up for six solid species, including two reactive fractions of particulate organic carbon (POC1 and POC2) and iodine (POI1 and POI2), particulate organic nitrogen and excess particulate iodine (XSI). Solutes include O_2, sulfate (SO_4^{2-}), H_2S, NH_4^+ and dissolved iodine (dI, corresponds to I^-). Parameter values, depth-dependent functions, kinetic rate laws, and rate terms applied in the model are listed in Table 2 and Tables S2–S5 in Supporting Information S1.

Constant fluxes (rain rates, RR) were applied for the solids at the upper boundary of the model ($x = 0$):

$$d_S \cdot (1-\Phi) \cdot \left(-D_B \cdot \frac{\partial S}{\partial t} + w \cdot S\right)\Big|_{x=0} = \mathrm{RR}_S \quad (3)$$

whereas constant concentrations corresponding to ambient bottom water values (P_{BW}) were used for the solutes:

$$P|_{x=0} = P_{BW} \quad (4)$$

A zero gradient condition was applied at the lower boundary ($x = L = 50$ cm) for all variables except NH_4^+ and dI in the OMZ:

$$\left.\frac{\partial S}{\partial x}\right|_{x=L} = 0 \qquad \left.\frac{\partial P}{\partial x}\right|_{x=L} = 0 \quad (5)$$

Table 2
Input Parameters of the Reaction-Transport Model and Key Model Outputs (See Tables S1–S4 in Supporting Information S1 for More Details)

Parameter	Description	Unit	Shelf	OMZ	Below OMZ	Generalized model
Input						
φ_0	Porosity at sediment-water interface	–	0.95	0.95	0.74	0.90
φ_f	Porosity at the low end of the modeled sediment column (50 cm)	–	0.85	0.85	0.63	0.80
BWO_2	Bottom water oxygen	μM	0.0	0.0	33.0	[a]
u_f	Burial velocity of solids after compaction (equals sedimentation rate, SR)	cm yr^{-1}	0.4	0.04	0.04	0.05, 0.1, 0.5
RRPOC1	Rain rate of POC1 to the seafloor	mmol m^{-2} d^{-1}	29.7	22.8	0.59	[b]
RRPOC2	Rain rate of POC2 to the seafloor	mmol m^{-2} d^{-1}	6.85	1.83	1.07	1.83
RRXSI	Rain rate of excess iodine to the seafloor	mmol m^{-2} d^{-1}	0.0	5.7×10^{-3}	5.7×10^{-3}	0.0
rNC	Molar nitrogen-to-carbon ratio in organic matter	mol mol^{-1}	3.80	3.80	3.80	3.80
rIN	Molar iodine-to-nitrogen ratio in organic matter	mmol mol^{-1}	1.10	1.10	1.10	1.10
kPOC1	Degradation constant for POC1	yr^{-1}	2.4	1.0	0.04	[c]
kPOC2	Degradation constant for POC2	yr^{-1}	2.5×10^{-3}	6.0×10^{-4}	4.0×10^{-5}	8.0×10^{-4}
kPOI1	Degradation constant for POI1	yr^{-1}	2.4	1.0	0.04	[d]
kPOI2	Degradation constant for POI2	yr^{-1}	5.0×10^{-3}	6.0×10^{-4}	4.0×10^{-5}	8.0×10^{-4}
KO_2NH_4	Rate constant for aerobic ammonium oxidation	$mmol^{-1}$ L yr^{-1}	1.0×10^6	1.0×10^6	1.0×10^6	1.0×10^6
KO_2dI	Rate constant for aerobic iodide oxidation and excess iodine precipitation	$mmol^{-1}$ L yr^{-1}	3.0×10^6	3.0×10^6	3.0×10^6	3.0×10^6
kXSIdiss	Rate constant for excess iodine dissolution	yr^{-1}	5.5×10^{-2}	5.5×10^{-2}	5.5×10^{-2}	5.5×10^{-2}
Output						
RRTI	Rain rate of total iodine	μmol m^{-2} d^{-1}	10.6	7.68	1.00	–
F_{iodide}	Iodide flux across the sediment-water interface (sum of diffusion, bioirrigation and bioturbation)	μmol m^{-2} d^{-1}	−9.38	−8.03	−0.17	–
I-MAR	Iodine mass accumulation rate at the lower end of the sediment column	μmol m^{-2} d^{-1}	1.16	0.36	0.846	–
I-BE	Iodine burial efficiency (MARI/RRTI)	%	11	5	84	–
$I:N_{burial}$	Iodine-to-nitrogen ratio at the lower end of the modeled sediment column	mmol mol^{-1}	0.84	1.44	3.13	–

Note. The input parameters of the generalized model runs are representative for burial velocities and organic carbon rain rates at continental margins (Burdige, 2007; Dale et al., 2015). Due to the limited range of bottom water oxygen concentrations observed on the Peruvian margin, the modeled range was limited to 0–100 μM.
[a] 1.0×10^{-5}, 1.0×10^{-3}, 1.0×10^{-1}, 1.0, 2.5, 5.0, 10, 25, 50, 100. [b] 0.2, 1, 2, 5, 10, 20, 30. [c] Calculated using an empirical relationship between kPOC1 and RRPOC1 on the slope within the OMZ and below the OMZ: kPOC1 = 0.037 × exp(324 × RRPOC1). [d] Equals kPOC1.

The linear increase in dissolved NH_4^+ and dI concentrations suggests that a non-zero gradient is more suitable for these variables in the OMZ:

$$\left.\frac{\partial S}{\partial x}\right|_{x=L} = -\frac{J_S}{\varphi \cdot D_S} \tag{6}$$

where J_S is the prescribed flux of S.

The model was solved using the solver for partial differential equations of MATHEMATICA v12 applying the Method-of-Lines approach. The model was integrated over time until a steady state was attained with a mass balance >99%.

2.3.2. Iodine-Specific Framework

In our model, iodine is delivered to the sediment surface in a fixed stoichiometry relative to carbon and nitrogen (Table 2). Organic carbon degradation in the sediment results in dissolved I^-(referred to as "dI" in the model), DIC and NH_4^+ release into the pore water according to the same fixed stoichiometry. Under low-oxygen conditions in the bottom water (shelf and OMZ), dI is transported across the SWI mainly by molecular diffusion.

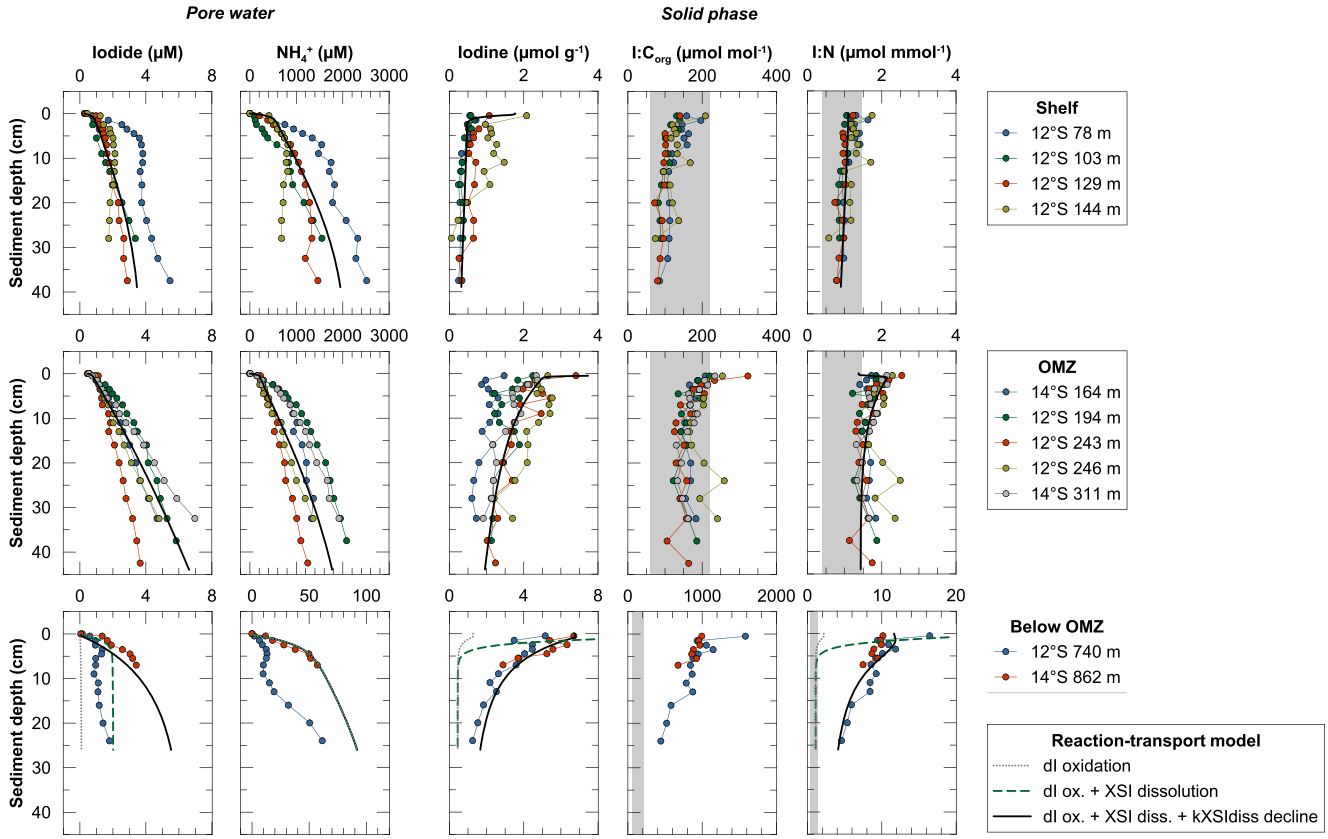

Figure 3. Pore water concentration profiles of I^- and NH_4^+ (two columns on the left) and solid phase profiles of iodine concentrations, iodine-to-organic carbon ($I:C_{org}$) and iodine-to-nitrogen (I:N) ratios (three columns on the right) for sediment cores from the shelf (upper row), the oxygen minimum zone (OMZ) (central row) and below the OMZ (lower row). Vertical gray arrays depict the I:C (Elderfield & Truesdale, 1980) and I:N in phytoplankton. The latter was calculated from I:C by assuming a Redfield-like C:N of 106:16. Solid and dashed lines represent the results of the reaction-transport modeling.

Because of the adverse effects of low oxygen concentrations and the presence of hydrogen sulfide on benthic fauna (Middelburg & Levin, 2009), bioirrigation plays a minor role in solute transport on the shelf and within the OMZ. Under oxic conditions in the surface sediment (below OMZ), pore water dI is oxidized with oxygen and precipitated as XSI according to the following kinetic rate law, where kO_2dI is the rate constant for dI oxidation and XSI precipitation:

$$R = kO_2dI \cdot [dI] \cdot [O_2] \quad (7)$$

The model was fit to our data, which are described in the next section. The data-model fit required additional considerations, which are discussed in detail in Section 4.2 in the Discussion.

3. Results

At most stations sampled during M136 and M137, oxygen concentrations in the bottom water were below the limit of detection of the Winkler method (2–3 μM) (Figure 2). At the shallowest shelf stations (78 m and 103 water depth), oxygen concentrations were mostly above the detection limit. The presence of oxygen in the water column on the shallow shelf was related to a coastal El Niño event, which took place in the weeks prior to the sampling campaign. The lower boundary of the OMZ (>5 μM of oxygen) was located at roughly 500 m water depth and BWO_2 at the sampling stations below the OMZ was approximately 20–40 μM (Figure 2).

Trends in the pore water profiles of I^- were generally similar to those of NH_4^+ at all study sites (Figure 3). On the shelf and within the OMZ, pore water I^- and NH_4^+ concentrations increased steeply within the uppermost 1–2 cm of the sediment and then increased more gradually toward the lower end of the core. On the shelf and within the OMZ, maximum I^- concentrations of 2–7 μM coincided with high NH_4^+ concentrations of the order

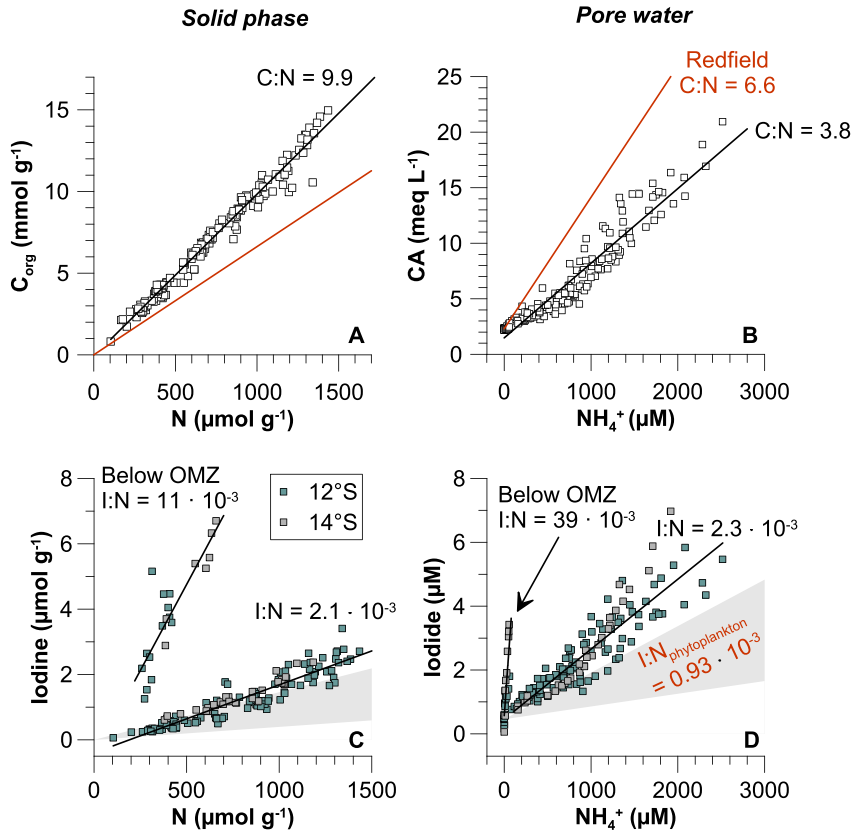

Figure 4. Cross plot of (a) C_{org} versus N, (b) carbonate alkalinity versus NH_4^+, (c) iodine versus N and (d) I^- versus NH_4^+. Data for 12°S and 14°S are shown in differing color in (c) and (d). Black lines represent linear regressions through data populations. Red lines and gray arrays depict C:N and I:N in phytoplankton, respectively. To make sure the pore water and solid phase C:N and I:N are comparable, the slope of regression of pore water data was multiplied by the ratio of the corresponding diffusion coefficients (NH_4^+:HCO_3^-, I^-:NH_4^+).

of 1,000–2,500 µM. Below the OMZ, maximum I^- concentrations were in the same range (~2–4 µM) but NH_4^+ concentrations were much lower (<70 µM) compared to the shallower sites. Pore water profiles of the shallowest sediment core (78 m) and sediment cores from below the OMZ were characterized by transient excursions at intermediate depths indicating that they were not in a steady state.

Solid phase iodine concentrations and $I:C_{org}$ were generally elevated at the surface and decreased with depth over the uppermost 5–10 cm (shelf and within the OMZ) or over the entire cored depth interval (below the OMZ) (Figure 3). On the shelf and within the OMZ, $I:C_{org}$ was mostly within the range reported for phytoplankton (140 ± 80 µmol mol^{-1}) (Elderfield & Truesdale, 1980) whereas below the OMZ, $I:C_{org}$ were highly elevated relative to phytoplankton (>1,000 µmol mol^{-1}). The downcore distribution of iodine-to-nitrogen ratios (I:N) was generally similar to that of $I:C_{org}$ although the deviation from phytoplankton values within and below the OMZ was somewhat higher.

4. Discussion

4.1. Stoichiometry of Carbon to Nitrogen to Iodine Turnover

Iodine is a biophilic element (Elderfield & Truesdale, 1980) meaning that it is taken up by phytoplankton in the surface ocean and remineralized upon organic matter degradation in the water column and sediments. To identify spatial patterns in sedimentary iodine turnover, it is therefore instructive to compare the stoichiometry of organic carbon to nitrogen to iodine in sediments and pore waters with that of phytoplankton (Figure 4).

Organic carbon and nitrogen are closely correlated with sediments across the entire Peruvian margin (Figure 4a). The slope of the linear regression (C:N = 9.9) is higher than both regionally observed (Bach et al., 2020;

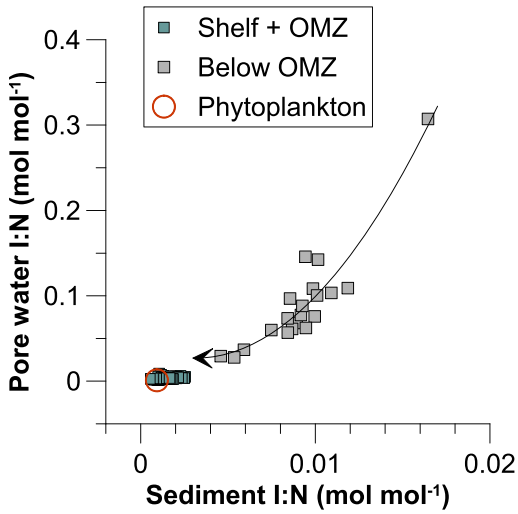

Figure 5. Pore water I:N versus solid phase I:N. The red circle depicts the I:N in phytoplankton. The black arrow represents a polynomial fit though data from the oxygen minimum zone pointing toward increasing sediment depth.

Sellner et al., 1983) and global average C:N ratios of marine phytoplankton (106:16 = 6.6) (Redfield, 1958). This observation confirms that nitrogen is preferentially remineralized whereas carbon is preferentially retained in the solid phase during early diagenesis (e.g., Froelich et al., 1988; Krom & Berner, 1981). The same trend is observed in the pore water (Figure 4b), whereby carbonate alkalinity (CA ≈ HCO_3^-; approximated by subtracting up to several mM of ΣH_2S, being mainly present as HS^- at pore water pH, from total alkalinity) and NH_4^+ (the most abundant nitrogen species in anoxic pore waters) are correlated and the slope of the linear regression (C:N = 3.8, corrected for differing diffusion coefficients of HCO_3^- and NH_4^+) is lower than the C:N of phytoplankton.

In sediment cores from the shelf and within the OMZ, solid phase iodine and nitrogen are correlated with I:N being consistent with or slightly higher (average C:N of 2.1×10^{-3}) than that of phytoplankton ($0.93 \pm 0.53 \times 10^{-3}$) (Elderfield & Truesdale, 1980) (Figure 4c). The ratio of I^- to NH_4^+ in the pore water of these cores is similar to the I:N of the solid phase (Figure 4d). These observations indicate that iodine is delivered with organic material and partly remineralized along with nitrogen during early diagenesis (Anschutz et al., 2000; Mackin et al., 1988; Ullman & Aller, 1985; Upstill-Goddard & Elderfield, 1988). As iodine and nitrogen behave similarly in anoxic Peruvian margin sediments and since no DIC data are available, we will mainly focus on I:N in the following discussion. However, it should be kept in mind that solid phase I:N can be converted to $I:C_{org}$ by applying a C:N ratio of 9.9 (Figure 4a).

Below the OMZ, both sediments and pore waters are characterized by highly elevated I:N compared to phytoplankton (Figures 4c and 4d), especially close to the sediment surface (Figure 5). The disproportionate increase in pore water I:N relative to solid phase I:N in Figure 5 suggests that some of the I^- enrichment relative to NH_4^+ may be related to aerobic or anaerobic NH_4^+ oxidation within oxic or nitrogenous surface sediments. In contrast, iodine enrichment relative to nitrogen in the solid phase cannot be explained by ammonia oxidation. However, it is fully consistent with prior studies on sedimentary iodine cycling (Francois, 1987; Harvey, 1980; Kennedy & Elderfield, 1987a, 1987b; Price & Calvert, 1977; Truesdale & Luther, 1995), which concluded that pore water I^- is oxidized to I_2 or HOI and precipitated through interaction with organic material in oxic surface sediments. Pore waters of anoxic subsurface sediments are also characterized by elevated I:N compared to phytoplankton (Figures 3, 4c, 4d, and 5), suggesting that some of the excess iodine precipitated within surface sediments (XSI relative to phytoplankton) is re-released to the pore water upon burial. Solid phase iodine concentrations decrease exponentially with sediment depth below the OMZ and subsurface sediments at the lower end of the sediment cores are still characterized by elevated $I:C_{org}$ and I:N relative to phytoplankton (Figure 3). Accordingly, XSI regeneration seems to be most intense close to the sediment surface but ceases during progressive burial.

4.2. Diagenetic Modeling of Sedimentary Iodine Cycling

The general modes of sedimentary iodine cycling under differing redox conditions identified in Section 4.1 are consistent with the interpretations of previous studies. However, in order to predict how BWO_2, organic carbon delivery and sedimentological factors determine benthic I^- release and sedimentary $I:C_{org}$ in the paleo-record, a more quantitative analyses of the data are required. To this end, we validated the above interpretations by simulating pore water profiles across the Peruvian continental margin using a numerical reaction-transport model. The data-model comparison makes several specific predictions regarding the diagenetic cycling of iodine:

First, I^- released from organic carbon during early diagenesis (referred to as dI in the model) is unlikely to be the sole source of iodine enrichment in surface sediment under oxic bottom waters. Specifically, the precipitation of dI in the surface sediment alone does not produce the characteristic dissolved and solid phase iodine and I:N maxima observed in sediments below the OMZ (model run "dI oxidation" in Figure 3). In order to generate those maxima, a fraction of XSI has to be re-dissolved and retained in the surface sediment by repeated dissolution and re-precipitation. We first implemented XSI re-dissolution by introducing the following kinetic rate law:

$$R = \mathrm{kXSIdiss} \cdot [\mathrm{XSI}] \quad (8)$$

where kXSIdiss is the rate constant for XSI dissolution. A combination of dI oxidation and XSI dissolution was able to generate dissolved and solid phase iodine enrichment at the sediment surface (model run "dI ox. + XSI dissolution" in Figure 3). However, this approach did not result in appropriate combinations of dissolved and solid phase iodine enrichment and the gentle decline in solid phase iodine and I:N with depth could not be reproduced. Instead, in this model configuration, XSI dissolved entirely within the modeled sediment column resulting in a decrease in solid phase iodine concentrations and I:N down to the values of the refractory organic carbon pool (POC2).

In order to achieve a more gradual decline in solid phase iodine concentrations and I:N, we applied a scaling function to the kinetic rate law of XSI dissolution so that kXSIdiss declines with depth:

$$R = \mathrm{fXSIdiss} \cdot \mathrm{kXSIdiss} \cdot [\mathrm{XSI}] \tag{9}$$

where

$$\mathrm{fXSIdiss} = 10^{-\mathrm{B2}} \cdot (x + \mathrm{B1})^{\mathrm{B2}} \tag{10}$$

where x is the depth and B1 and B2 are fitting parameters. By choosing appropriate values for B1 and B2 (Table 1), all pore water and solid phase profiles could be reproduced, including the gentle decline in solid phase iodine below the OMZ (model run "dI ox. + XSI diss. + kXSIdiss decline" in Figure 3). From a mechanistic point of view, Equations 9 and 10 imply that the reactivity of XSI bound to organic material decreases with time after deposition. In other words, the extent to which XSI is buried beyond the depth of active iodine redox cycling also depends on burial velocity (i.e., sedimentation rate).

Fitting the solid phase profiles of stations within and below the OMZ requires an additional flux of solid phase iodine to the sediment surface besides the one associated with POC1 and POC2. This can be achieved by either increasing the proportion of iodine in POC1 and POC2 or by adopting a rain rate of XSI to the sediment surface (Table 2). Given that much of the organic material accumulating within and below the OMZ originates from areas further up on the shelf and slope (Dale et al., 2015), it is likely that the XSI delivered to these sites is also derived from downslope transport.

The steep gradients of dI within the topmost cm of shelf sediments (Figure 3) is caused by a high rain rate of reactive organic material (RRPOC1 and RRPOI) (Table 2), which is remineralized close the sediment surface. Since the bottom water and surface sediments were anoxic at these sites during the sampling campaign, much of the dI is lost via diffusion across the SWI. Accordingly, the model yields a high benthic dI flux (-9.4 μmol m^{-2} d^{-1}) and a low iodine burial efficiency for shelf sediments (percentage of delivered iodine that is buried; 11%) (Table 2; a comparison with benthic dI fluxes calculated based on pore water profiles is contained in the Electronic Supplement). In contrast, less organic material is delivered to slope sediments below the OMZ and the majority of the dI remineralized is re-oxidized within the surface sediment. Therefore, little of the delivered iodine is lost across the SWI (-0.17 μmol m^{-2} d^{-1}) resulting in a high burial efficiency of 84% (Table 2). Due to intense iodine redox cycling (precipitation and partial re-dissolution of XSI) in the surface sediment below the OMZ, I:N at the lower end of the sediment column ($I:N_{burial}$) is considerably higher compared to phytoplankton and sediments underlying anoxic bottom water (Table 2).

Our reaction-transport model provides a quantitative framework for explaining how organic carbon rain rate, BWO_2 and sedimentation rate determine the magnitude of the benthic I^- efflux and sedimentary I:N (or $I:C_{org}$). In the following sections, we will conduct sensitivity tests with a generalized version of the model to predict the environmental circumstances under which significant sedimentary I^- release and thus associated anomalies in the water column are to be expected, along with $I:C_{org}$ paleo-signatures. We include additional previously published data as part of the model validation and discussion, specifically from the Benguela Upwelling System and the northeast Pacific Ocean (Table 3). Notably, while several additional diagenetic and water column iodine cycling studies are included in our broader discussion, only those studies shown in Table 3 reported the necessary BWO_2, sedimentation rate, and $I:C_{org}$ required for direct inclusion in our data-model comparison. We note that those data sets for the Peruvian margin, Benguela Upwelling System and northeast Pacific cover end-member low O_2 environments. Model calibration against similar data from intermediate and high O_2 environments is necessary for broader global applications.

4.3. Iodine as a Tracer for Benthic Inputs to OMZ Waters

Substantial benthic I^- effluxes have been inferred in the OMZs of the northeastern and southeastern equatorial Pacific and the Arabian Sea based on the presence of excess dissolved iodine (as I^-) in the water column (Cutter

Table 3
Reference Data for Sediments From the Benguela Upwelling System and Northeast Pacific Ocean Shown in Figures 8 and 9

Site	Latitude	Longitude	Water depth (m)	Bottom water oxygen (μM)	Sedimentation rate (cm yr^{-1})	Organic carbon rain rate[a] (mmol C m^{-2} day^{-1})	I:$C_{org, burial}$[b] (μmol mol^{-1})	Reference
Northeast Pacific								
01mc	48°45.95′N	125°29.57′W	120	105	0.0395	0.947	520	McKay et al. (2007)
04mc	49°00.71′N	126°49.82′W	407	44	0.0007	0.004	567	McKay et al. (2007)
06bc	48°58.73′N	126°52.68′W	720	18	0.0016	0.037	284	McKay et al. (2007)
09mc	48°54.76′N	126°53.44′W	920	13	0.0047	0.166	615	McKay et al. (2007)
02mc	49°12.81′N	127°18.57′W	1,340	18	0.0063	0.245	946	McKay et al. (2007)
05bc	49°07.91′N	127°33.12′W	1,750	53	0.0046	0.085	851	McKay et al. (2007)
Benguela Upwelling System								
CIR178B	22°35.00′S	14°05.00′E	108	18	0.065	6.530	236	Price and Calvert (1977)[c,d]
CIR179A	22°35.80′S	13°55.80′E	123	33	0.065	1.020	208	Price and Calvert (1977)[c,d]
CIR176A	22°57.00′S	14°13.90′E	127	21	0.103	8.36	255	Price and Calvert (1977)[d,e]
CIR175	22°56.40′S	13°59.60′E	134	42	0.103	10.3	236	Price and Calvert (1977)[d,e]
CIR150	25°10.60′S	13°18.50′E	1,358	170	0.110	3.55	634	Price and Calvert (1977)[e,f]

[a]Approximated using the organic carbon concentration at the sediment surface and the mass accumulation rate (MAR). For cores from the northeast Pacific, MAR was approximated from sedimentation rates assuming a porosity of 0.8 and a dry sediment density of 2.5 g cm^{-3}. [b]Refers to the lower end of each profile. [c]Oxygen data inferred from figures. [d]Sedimentation rate from Veeh et al. (1974). [e]Oxygen data from Scripps Institution of Oceanography (1978). [f]Sedimentation rate approximated from Chuang et al. (2022).

et al., 2018; Farrenkopf & Luther, 2002; Moriyasu et al., 2020; Shaikh et al., 2023). Due to its low reactivity under anoxic and nitrogenous conditions (i.e., as opposed to other sediment-derived compounds such as dissolved ferrous Fe) (Heller et al., 2017; Scholz et al., 2016), I^- has been proposed as a tracer for sediment inputs to OMZ waters (Cutter et al., 2018).

We evaluate the utility of iodine as a biogeochemical tracer for sediment inputs by comparing water column excess dissolved iodine concentrations measured in our study area during two different sampling campaigns (see Figure 1 for sampling locations) with our model-derived dI fluxes across the SWI and iodine burial efficiencies (fraction of iodine delivered that is buried) (Figure 6). The highest excess dissolved iodine concentrations (up to ~2,000 nM) were observed in the anoxic water column between 50 and 350 m water depth during the GEOTRACES cruise GP16 (Figure 6), which took place in October–December 2013 (Cutter et al., 2018). This depth range coincides with the area, where the highest benthic dI fluxes and lowest burial efficiencies were obtained from the reaction-transport model (Figure 6). Below 400 m water depth, excess dissolved iodine concentrations are lower (≤220 nM), consistent with a small benthic dI flux (Figure 6). The excellent match between high excess dissolved iodine in the water column and intense benthic I^- release underscores the utility of dissolved seawater iodine as a tracer for benthic solute inputs to the OMZ.

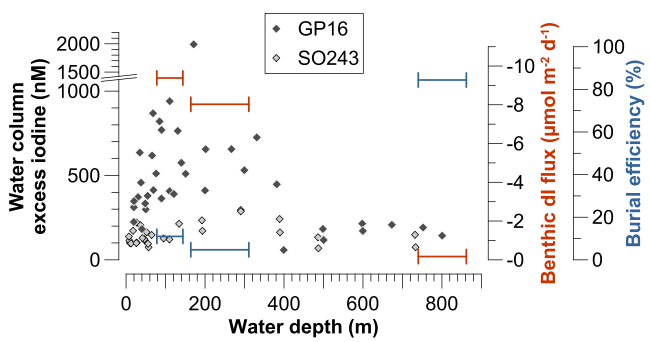

Figure 6. Water column excess dissolved iodine concentrations measured on samples from GEOTRACES cruise GP16 (Cutter et al., 2018) and RV Sonne cruise SO243 (Rapp et al., 2020) as well as model-derived benthic dI fluxes (red bars) and iodine burial efficiencies (blue bars) for sediment cores from the shelf, within the oxygen minimum zone (OMZ) and below the OMZ plotted against water depth. Excess dissolved iodine corresponds to the sum of I^- and IO_3^- minus the average iodine concentration in seawater of 470 nM.

Another published iodine data set was obtained on RV Sonne cruise SO243 (October 2015), which took place during the 2015/2016 El Niño Event (Stramma et al., 2016). Less reducing conditions were observed in the water column overlying the Peruvian shelf at 12°21′S, as indicated by higher oxygen concentrations and a deeper oxycline (Stramma et al., 2016). Excess dissolved iodine concentrations were much lower than during GEOTRACES cruise GP16 (≤300 nM) and essentially uniform in the upper 900 m of the water column (Figure 6) (Rapp et al., 2020). Apparently, shelf oxygenation had initiated shallow iodine redox cycling in the surface sediment and, therefore, led to diminished benthic I^- release. This interpretation is supported by earlier studies on the Peruvian margin, which demonstrated that shelf

oxygenation may shut down benthic iron fluxes and modulate trace metal diagenesis (Noffke et al., 2012; Scholz et al., 2011). Furthermore, occasional shelf oxygenation and non-steady state diagenesis of iodine can explain the curved shape of pore water profiles (78 m station) and somewhat elevated particulate iodine at the sediment surface at the shelf stations (Figure 3).

Applying a generalized version of the reaction transport-model over the range of organic carbon rain rates, BWO_2 and sedimentation rates typically prevailing at continental margins (Table 2, Figure 7) (Burdige, 2007; Dale et al., 2015) illustrates the relative effects of these three key-parameters on sedimentary I^- release (Figure 7, left column). High benthic dI fluxes require a high rain rate of reactive organic material, which is remineralized close to the SWI. BWO_2 becomes increasingly important at high sedimentation rates (Figure 7, upper row). Under conditions of rapid burial, a greater proportion of organic matter remineralization and I^- release takes place deeper in the sediment. The distance over which I^- may diffuse toward the SWI then depends on BWO_2 and thus the oxygen penetration depth (Cai & Sayles, 1996). It should be noted that high rates of primary productivity, low oxygen concentrations in the water column and high rates of organic carbon rain to the seafloor are interconnected factors in OMZs. Therefore, the overall sedimentation rate may be of particular importance for the magnitude of the benthic efflux in those settings.

The Peruvian shelf features fairly high sedimentation rates and some of the highest organic carbon rain rates published to date (Burdige, 2007; Dale et al., 2015). Therefore, dI fluxes from sediments in this area (reaction-transport model: -9.4 μmol m^{-2} d^{-1} (Table 2); calculated based on pore water profiles: -6 to -19 μmol m^{-2} d^{-1} (Table S6 in Supporting Information S1)) are likely to be at the upper end of the range at open-marine continental margins. Considering the large error of benthic flux calculations, these benthic iodine fluxes are similar to those reported for shelf sediments in the Arabian Sea (-14 to -43 μmol m^{-2} d^{-1}) (Shaikh et al., 2023) and estuarine sediments in the eastern USA (-5 to -41 μmol m^{-2} d^{-1}) (Ullman & Aller, 1980). Lower, yet still significant benthic I^- fluxes (∼-3 μmol m^{-2} d^{-1}) were reported for north Atlantic deep-sea sediments by Kennedy and Elderfield (1987b). Furthermore, notable excess dissolved iodine (order of a few nM) was found in bottom waters in the deep north Pacific (Moriyasu et al., 2023; Tsunogai, 1971). These findings in deep-sea settings are in apparent conflict with our model results. Importantly, however, mass balance constraints (rain rate of iodine equals iodine efflux and burial) (Table 2) dictate that most of the liberated iodine from deep-sea sediments in the north Atlantic must be scavenged and re-deposited close to the source (Kennedy & Elderfield, 1987b). Because of the prescribed upper boundary conditions (dI in the bottom water), I^- removal at the sediment surface and in the bottom water cannot be differentiated in our reaction-transport model. In contrast to the study of Kennedy and Elderfield (1987b), however, re-deposition is not required to balance iodine delivery and removal at our study sites (Table 2). In other words, the benthic efflux determined for the Peruvian margin represents a net iodine loss to the water column, which is consistent with the iodine plume emanating from shelf sediments observed by Cutter et al. (2018).

4.4. Evaluation of Iodine-To-Organic Carbon Ratios as a Paleo-Redox Proxy

Due to iodine redox cycling, surface sediments underneath oxic bottom waters are typically characterized by elevated $I:C_{org}$ relative to phytoplankton (Price & Calvert, 1973, 1977). Therefore, $I:C_{org}$ has been employed as a paleo-redox proxy (Calvert & Pedersen, 1993; Hendy & Pedersen, 2005; Martinez-Ruiz et al., 2000; Pedersen et al., 1988; Zhou et al., 2017). However, the integrity of the $I:C_{org}$ proxy is potentially compromised by the fact that much of the iodine enrichment disappears over the upper tens of cm of the sediment column during shallow burial (Figure 3). Furthermore, deep-seated pore fluids in drill cores and at cold seeps originating from deeply buried organic matter-rich formations are known to be strongly enriched in I^- (several hundred μM) (Lu et al., 2008; Scholz et al., 2010). It is therefore possible that ongoing I^- release during burial diagenesis changes the $I:C_{org}$ of the remaining organic matter. In agreement with such a scenario, Martin et al. (1993) reported decreasing $I:C_{org}$ with depth in drill cores from ODP Leg 112 to the Peruvian margin (see Figure 1 for the location of drill sites). However, their sample number was limited and no shallow sediment data for comparison were available. We further evaluate the impact of deep-seated diagenesis by comparing our pore water data for shallow MUCs with pore water data from ODP Leg 112 (Figure 8) (Martin et al., 1993). Despite much higher I^- and NH_4^+ concentrations in deep-seated compared to shallow pore waters, the trends of I^- to NH_4^+ are largely consistent above and below 500 m water depth (roughly corresponding to the present-day lower boundary of the OMZ). This observation may indicate that ongoing diagenesis during deep burial does not alter the I:N signature that was generated during early diagenesis. Whether this finding can be extrapolated to $I:C_{org}$ or if it is instead preferable to use I:N as a paleo-redox proxy needs to be addressed in future studies.

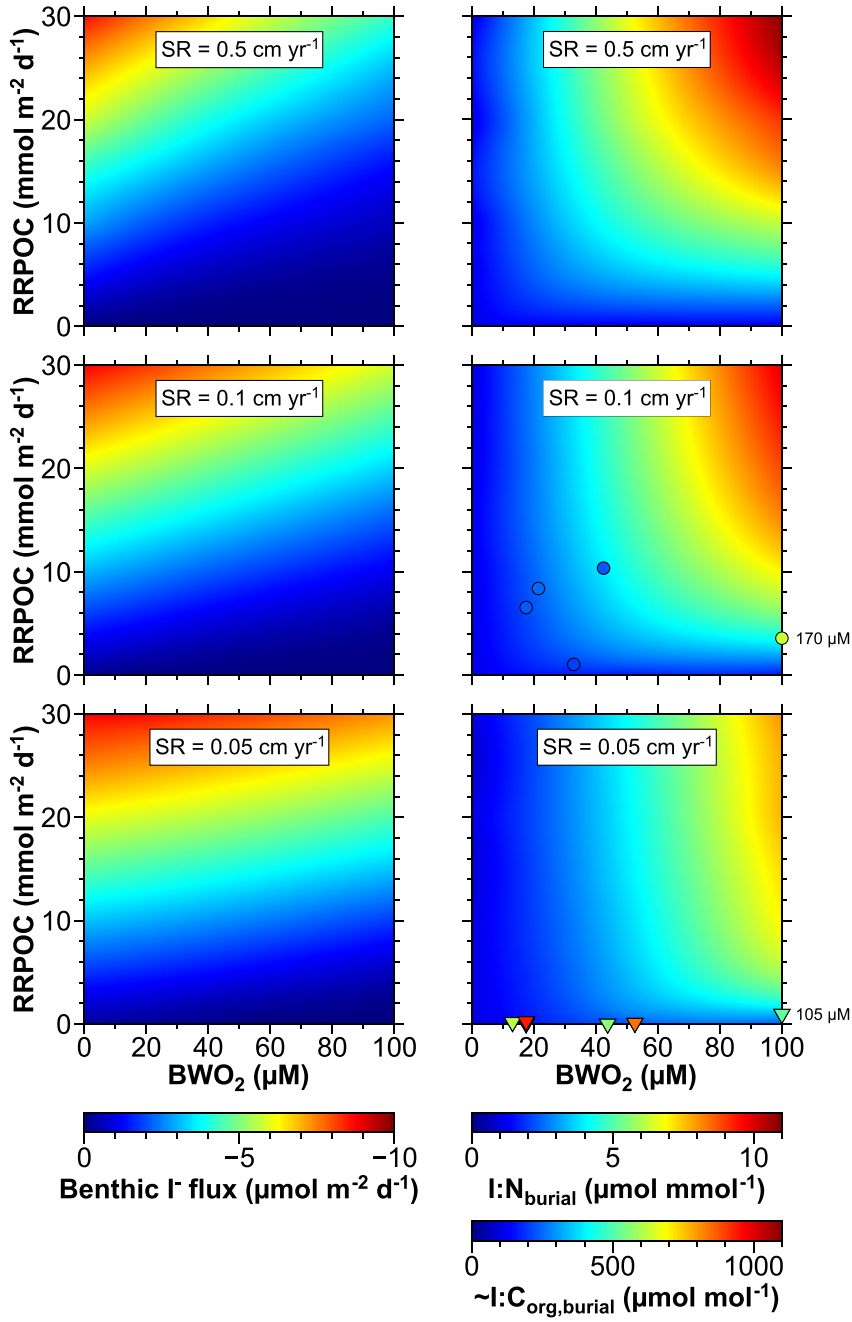

Figure 7. Results of sensitivity tests using the reaction-transport model: Benthic I^- flux (left column) and $I:N_{burial}$ (i.e., at the lower end of each modeled profile) (right column) as a function of bottom water oxygen concentration (BWO_2) and the rain rate of reactive organic matter that is readily degradable (RRPOC; corresponding to RRPOC1 in Table 2). The model was run with three different sedimentation rates (SR: 0.05, 0.1, 0.5 cm yr^{-1}) covering the range typical for continental margins. Colored circles and triangles depict sedimentary $I:C_{org}$ measured at the lower end of sediment cores from the Benguela Upwelling System off Namibia (Price & Calvert, 1977) and the northeast Pacific Ocean off Vancouver Island (McKay et al., 2007), respectively (see Table 3 for details). Sedimentary I:N and $I:C_{org}$ were converted by assuming a C:N of 9.9 (see Figure 4). Symbols plotting on the *y*-axis have a BWO_2 above 100 µM; the actual concentration is shown next to the symbol.

Another theoretical limitation of the $I:C_{org}$ redox-proxy is that bottom water oxygen is only one control on the $I:C_{org}$ or I:N with organic carbon rain rate and sedimentation rate being equally important (Figure 7). According to our model-derived framework, the highest $I:C_{org}$ at the lower end of the modeled sediment column (hereafter referred to as $I:C_{org,\ burial}$) should be generated at high BWO_2 and high organic carbon rain rates (Figure 7, right

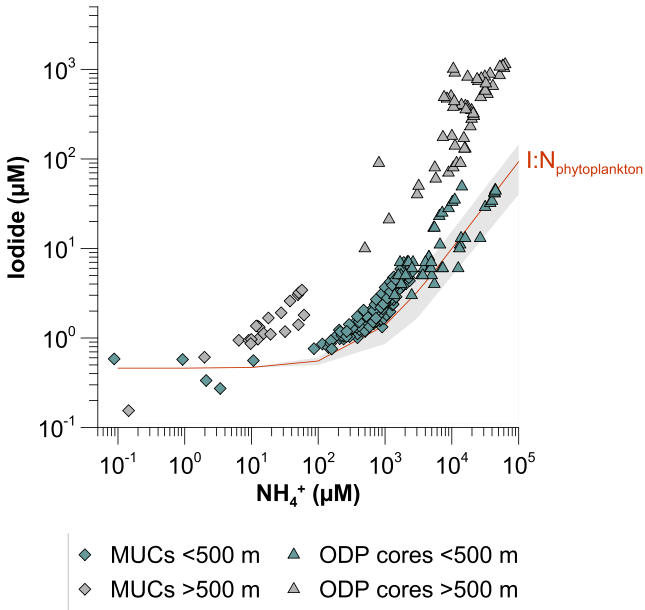

Figure 8. Pore water I^- versus NH_4^+ in shallow pore waters of MUCs and deep pore waters of drill cores from Ocean Drilling Program Leg 112. Note logarithmic scales. The gray array depicts the I:N in phytoplankton.

column). It should be noted that this combination is unlikely to be common in the ocean because sedimentary environments in highly productive settings (e.g., upwelling areas) are typically characterized by oxygen deficient bottom waters. However, it is still possible that $I:C_{org,\ burial}$ at a given BWO_2 may vary over a broad range (0–1,100 µmol mol^{-1}) as a function of differing organic carbon rain and sedimentation rates (along the *y*-axis in Figure 7, right column).

To test the validity of our model-derived framework, we compiled published data of $I:N_{burial}$ (approximated from I:C at the lower end of sediment cores assuming a sedimentary C:N of ∼10 (see Figure 4)), organic carbon rain rate, bottom water oxygen and sedimentation rate for the Benguela upwelling system and the northeast Pacific margin (Table 3; Figure 7, right column) (McKay et al., 2007; Price & Calvert, 1977). The data were roughly grouped according to sedimentation rate (Benguela upwelling: ∼0.1 cm yr^{-1}; northeast Pacific: ≤0.05 cm yr^{-1}) (Table 3). It should be noted that published organic carbon rain rates are not strictly comparable to those used in the model since the latter represents only the reactive fraction of the organic material raining onto the seafloor (RRPOC1 in Table 2). Despite this limitation, the data for the Benguela system are generally in good agreement with the I:N predicted by the model. One deviating data point (low $I:N_{burial}$ at a BWO_2 of 42 µM) can be explained by high amplitude fluctuations in bottom water oxygen on the Namibian shelf (e.g., Mohrholz et al., 2008). Kossack et al. (2023) measured highly variable oxygen concentrations close to the coring location of Price and Calvert (1977) in September 2019 (∼30 µM) and February 2022 (below limit of detection). Therefore, it is likely that the oxygen concentration measured in the Benguela system by Price and Calvert (1977) was not representative of the average oxygen concentration that controlled sedimentary iodine cycling at this site.

With the exception of one data point (shallowest shelf site with BWO_2 of 105 µM) (Table 3), data from the northeast Pacific are generally not consistent with the model-derived framework (Figure 7, right column). Specifically, $I:N_{burial}$ is mostly too high for the given BWO_2 and organic carbon rain rate. The corresponding sediment cores were retrieved along a transect covering the shelf and slope from 120 to 1,750 m water depth (Figure 9). In conflict with the rationale of the $I:C_{org}$ redox proxy (Zhou et al., 2017), $I:C_{org,\ burial}$ increases with water depth despite decreasing BWO_2. This trend could be explained by downslope transport of organic material and XSI as inferred above for the Peruvian slope based on the results of the reaction-transport model (see RRXSI in Table 2 and Section 4.2). Off-shelf and downslope transport of refractory organic material is a ubiquitous process at continental margins (e.g., Dale et al., 2015; Inthorn et al., 2006; Jahnke et al., 1990). Furthermore, sluggish re-oxidation and scavenging of sediment-derived I^- in the benthic boundary layer (see Section 4.3) may also contribute to the lateral displacement of XSI. Quantifying the contribution of those processes to sedimentary $I:C_{org}$ requires further investigation of sediment trap material and near-bottom suspended particles.

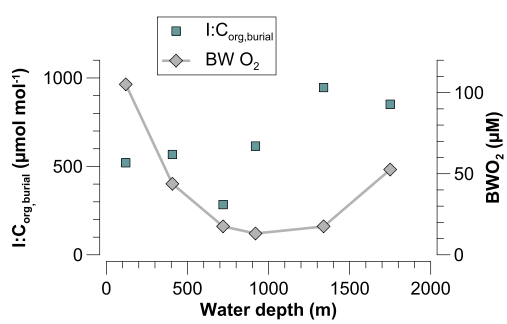

Figure 9. Sedimentary $I:C_{org,\ burial}$ (i.e., measured at the lower end of each core) and bottom water oxygen concentration (BWO_2) for sediment cores (30–50 cm long) from the northeast Pacific Ocean off Vancouver Island plotted against water depth (data from McKay et al. (2007)).

5. Conclusions

We investigated sedimentary iodine cycling across the Peruvian continental margin. A numerical reaction-transport model was used to evaluate how bottom water oxygen as well as organic carbon rain rate and sedimentation rate determine the benthic flux of I^- to the bottom water and the solid phase I:N or $I:C_{org}$ that enters the paleo-record. The validity of our data interpretation and general model setup was evaluated by fitting the model to our pore water and solid phase data and by comparing our results with previously published water column iodine distributions in the Peru upwelling and sedimentary $I:C_{org}$ at other continental margins. Our main findings are

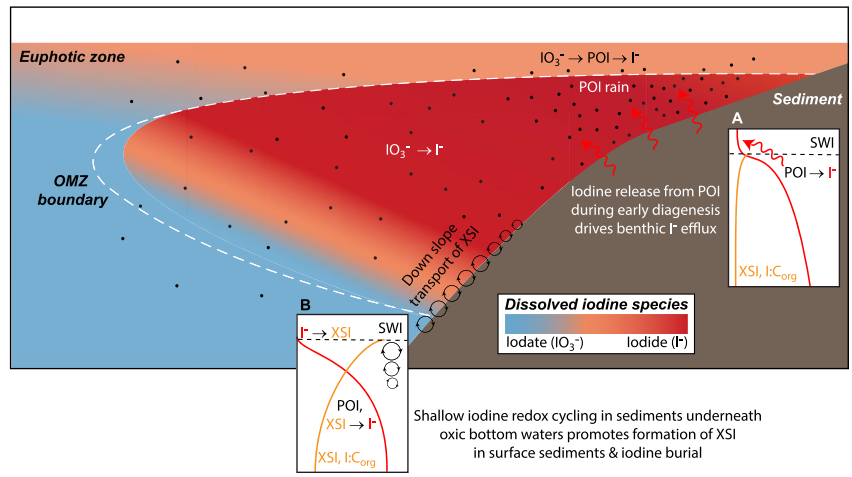

Figure 10. Conceptual model illustrating iodine cycling across the Peruvian continental margin. The schematized pore water profiles depict two end member situations: (A) Release of I^- across the sediment-water interface (sinuous arrows) from anoxic sediments underneath highly productive surface waters and anoxic bottom waters. (B) Shallow iodine redox cycling (I^- oxidation, formation of XSI, XSI re-dissolution and partial burial) in sediments underneath oxic bottom waters.

summarized in a conceptual model illustrating two endmember situations (A: anoxic bottom water, B: oxic bottom water) of iodine cycling in continental margin sediments (Figure 10).

A: Iodine is taken up by phytoplankton in the surface ocean and delivered to the sediment surface with organic material (POI). During early diagenesis, POI is remineralized and I^- is released into the pore water along with NH_4^+. Under anoxic conditions, much of the I^- delivered is recycled across the SWI. The benthic I^- flux is mainly a function of the organic carbon and thus POI rain rate to the seafloor. According to our findings, excess dissolved iodine in the water column can generally be used as a tracer for benthic fluxes to the OMZ from anoxic sediments with high organic carbon turnover.

B: Under oxic conditions in the bottom water and surface sediment, pore water dissolved I^- is oxidized and scavenged through the interaction of I_2 or HOI with fresh organic material. Due to this process, surface sediments are enriched in iodine (presence of XSI) compared to the $I:C_{org}$ of phytoplankton. Much of the XSI re-dissolves during early diagenesis and only a fraction is buried. The fraction of XSI buried and $I:C_{org,\ burial}$ recorded in sedimentary archives generally increases with bottom water oxygen. However, multiple combinations of BWO_2, organic carbon rain rate and sedimentation rate can lead to identical $I:C_{org,\ burial}$, which limits the utility of $I:C_{org}$ as a quantitative oxygenation proxy. Furthermore, multiple lines of evidence suggest that XSI may also be laterally transported at continental margins, either associated with organic material or by repeated oxidation-reduction cycles close to the SWI. This potential "iodine shuttle" may further complicate the $I:C_{org}$ paleo-record.

Besides the implications outlined above, our findings may be useful to better constrain the global ocean's iodine mass balance and how it has varied in the past as a function of marine productivity and ocean oxygenation.

Data Availability Statement

The data reported in this article are available at the online data repository PANGAEA (Scholz & Hardisty, 2023, https://doi.pangaea.de/10.1594/PANGAEA.963218; Sommer & Dale, 2021, https://doi.pangaea.de/10.1594/PANGAEA.928280).

References

Anschutz, P., Sundby, B., Lefrançois, L., Luther, G. W., & Mucci, A. (2000). Interactions between metal oxides and species of nitrogen and iodine in bioturbated marine sediments. *Geochimica et Cosmochimica Acta*, *64*(16), 2751–2763. https://doi.org/10.1016/s0016-7037(00)00400-2

Bach, L. T., Paul, A. J., Boxhammer, T., Von Der Esch, E., Graco, M., Schulz, K. G., et al. (2020). Factors controlling plankton community production, export flux, and particulate matter stoichiometry in the coastal upwelling system off Peru. *Biogeosciences*, *17*(19), 4831–4852. https://doi.org/10.5194/bg-17-4831-2020

Bohlen, L., Dale, A. W., Sommer, S., Mosch, T., Hensen, C., Noffke, A., et al. (2011). Benthic nitrogen cycling traversing the Peruvian oxygen minimum zone. *Geochimica et Cosmochimica Acta*, *75*(20), 6094–6111. https://doi.org/10.1016/j.gca.2011.08.010

Acknowledgments
We thank the officers and crew of RV Meteor during M136 and M137 for supporting our work at sea as well as the technician team at GEOMAR (Anke Bleyer, Bettina Domeyer, Regina Surberg) for assistance on board and in the laboratories. This study was supported by the German Research Foundation through the Emmy Noether Research Group ICONOX (Iron Cycling in Continental Margin Sediments and the Nutrient and Oxygen Balance of the Ocean) and Collaborative Research Center 754 (Climate-Biogeochemistry Interactions in the Tropical Ocean). DSH acknowledges US NSF-OCE 1829406 and laboratory assistance from Nick Battjes. Constructive comments by two reviewers helped us to improve the manuscript. Open Access funding enabled and organized by Projekt DEAL.

Burdige, D. J. (2007). Preservation of organic matter in marine sediments: Controls, mechanisms, and an imbalance in sediment organic carbon budgets? *Chemical Reviews*, *107*(2), 467–485. https://doi.org/10.1021/cr050347q

Cai, W.-J., & Sayles, F. L. (1996). Oxygen penetration depths and fluxes in marine sediments. *Marine Chemistry*, *52*(2), 123–131. https://doi.org/10.1016/0304-4203(95)00081-x

Calvert, S. E., & Pedersen, T. F. (1993). Geochemistry of recent oxic and anoxic marine-sediments - Implications for the geological record. *Marine Geology*, *113*(1–2), 67–88. https://doi.org/10.1016/0025-3227(93)90150-t

Chuang, P.-C., Anderson, C. H., Kossack, M., Fabian, J., Su, C.-C., Vosteen, P., et al. (2022). Nutrient turnover by large sulfur bacteria on the Namibian mud belt during the low productivity season. *Frontiers in Marine Science*, *9*, 929913. https://doi.org/10.3389/fmars.2022.929913

Cutter, G. A., Moffett, J. W., Nielsdóttir, M. C., & Sanial, V. (2018). Multiple oxidation state trace elements in suboxic waters off Peru: In situ redox processes and advective/diffusive horizontal transport. *Marine Chemistry*, *201*, 77–89. https://doi.org/10.1016/j.marchem.2018.01.003

Dale, A. W., Sommer, S., Lomnitz, U., Bourbonnais, A., & Wallmann, K. (2016). Biological nitrate transport in sediments on the Peruvian margin mitigates benthic sulfide emissions and drives pelagic N loss during stagnation events. *Deep Sea Research Part I: Oceanographic Research Papers*, *112*, 123–136. https://doi.org/10.1016/j.dsr.2016.02.013

Dale, A. W., Sommer, S., Lomnitz, U., Montes, I., Treude, T., Liebetrau, V., et al. (2015). Organic carbon production, mineralization and preservation on the Peruvian margin. *Biogeosciences*, *12*(5), 1537–1559. https://doi.org/10.5194/bg-12-1537-2015

Dalsgaard, T., Thamdrup, B., Farías, L., & Revsbech, N. P. (2012). Anammox and denitrification in the oxygen minimum zone of the eastern South Pacific. *Limnology and Oceanography*, *57*(5), 1331–1346. https://doi.org/10.4319/lo.2012.57.5.1331

Elderfield, H., & Truesdale, V. W. (1980). On the biophilic nature of iodine in seawater. *Earth and Planetary Science Letters*, *50*(1), 105–114. https://doi.org/10.1016/0012-821x(80)90122-3

Farrenkopf, A. M., Dollhopf, M. E., Chadhain, S. N., Luther, G. W., & Nealson, K. H. (1997). Reduction of iodate in seawater during Arabian Sea shipboard incubations and in laboratory cultures of the marine bacterium Shewanella putrefaciens strain MR-4. *Marine Chemistry*, *57*(3–4), 347–354. https://doi.org/10.1016/s0304-4203(97)00039-x

Farrenkopf, A. M., & Luther, III, G. W. (2002). Iodine chemistry reflects productivity and denitrification in the Arabian Sea: Evidence for flux of dissolved species from sediments of western India into the OMZ. *Deep Sea Research Part II: Topical Studies in Oceanography*, *49*(12), 2303–2318. https://doi.org/10.1016/s0967-0645(02)00038-3

Feng, X., & Redfern, S. A. T. (2018). Iodate in calcite, aragonite and vaterite $CaCO_3$: Insights from first-principles calculations and implications for the I/Ca geochemical proxy. *Geochimica et Cosmochimica Acta*, *236*, 351–360. https://doi.org/10.1016/j.gca.2018.02.017

Francois, R. (1987). The influence of humic substances on the geochemistry of iodine in nearshore and hemipelagic marine sediments. *Geochimica et Cosmochimica Acta*, *51*(9), 2417–2427. https://doi.org/10.1016/0016-7037(87)90294-8

Froelich, P. N., Arthur, M. A., Burnett, W. C., Deakin, M., Hensley, V., Jahnke, R., et al. (1988). Early diagenesis of organic matter in Peru continental margin sediments: Phosphorite precipitation. *Marine Geology*, *80*(3–4), 309–343. https://doi.org/10.1016/0025-3227(88)90095-3

Glock, N., Liebetrau, V., & Eisenhauer, A. (2014). I/Ca ratios in benthic foraminifera from the Peruvian oxygen minimum zone: Analytical methodology and evaluation as a proxy for redox conditions. *Biogeosciences*, *11*(23), 7077–7095. https://doi.org/10.5194/bg-11-7077-2014

Gutiérrez, D., Enríquez, E., Purca, S., Quipúzcoa, L., Marquina, R., Flores, G., & Graco, M. (2008). Oxygenation episodes on the continental shelf of central Peru: Remote forcing and benthic ecosystem response. *Progress in Oceanography*, *79*(2–4), 177–189. https://doi.org/10.1016/j.pocean.2008.10.025

Harvey, G. R. (1980). A study of the chemistry of iodine and bromine in marine sediments. *Marine Chemistry*, *8*(4), 327–332. https://doi.org/10.1016/0304-4203(80)90021-3

Heller, M. I., Lam, P. J., Moffett, J. W., Till, C. P., Lee, J.-M., Toner, B. M., & Marcus, M. A. (2017). Accumulation of Fe oxyhydroxides in the Peruvian oxygen deficient zone implies non-oxygen dependent Fe oxidation. *Geochimica et Cosmochimica Acta*, *211*, 174–193. https://doi.org/10.1016/j.gca.2017.05.019

Hendy, I. L., & Pedersen, T. F. (2005). Is pore water oxygen content decoupled from productivity on the California Margin? Trace element results from Ocean Drilling Program Hole 1017E, San Lucia slope, California. *Paleoceanography*, *20*(4), PA4026. https://doi.org/10.1029/2004PA001123

Hong, H., & Kester, D. R. (1986). Redox state of iron in the offshore waters of Peru. *Limnology and Oceanography*, *31*(3), 512–524. https://doi.org/10.4319/lo.1986.31.3.0512

Inthorn, M., Wagner, T., Scheeder, G., & Zabel, M. (2006). Lateral transport controls distribution, quality, and burial of organic matter along continental slopes in high-productivity areas. *Geology*, *34*(3), 205–208. https://doi.org/10.1130/g22153.1

Jahnke, R. A., Reimers, C. E., & Craven, D. B. (1990). Intensification of recycling of organic matter at the sea floor near ocean margins. *Nature*, *348*(6296), 50–54. https://doi.org/10.1038/348050a0

Kennedy, H. A., & Elderfield, H. (1987a). Iodine diagenesis in non-pelagic deep-sea sediments. *Geochimica et Cosmochimica Acta*, *51*(9), 2505–2514. https://doi.org/10.1016/0016-7037(87)90301-2

Kennedy, H. A., & Elderfield, H. (1987b). Iodine diagenesis in pelagic deep-sea sediments. *Geochimica et Cosmochimica Acta*, *51*(9), 2489–2504. https://doi.org/10.1016/0016-7037(87)90300-0

Kossack, M., Scholz, F., Anderson, C. H., Vosteen, P., Chih-Chieh, S., Mohrholz, V., & Zabel, M. (2023). Sedimentary molybdenum and uranium cycling under seasonally contrasting redox conditions on the Namibian Shelf. *Geochimica et Cosmochimica Acta*, *358*, 174–191. https://doi.org/10.1016/j.gca.2023.08.014

Krom, M. D., & Berner, R. A. (1981). The diagenesis of phosphorus in a nearshore marine sediment. *Geochimica et Cosmochimica Acta*, *45*(2), 207–216. https://doi.org/10.1016/0016-7037(81)90164-2

Lam, P., Lavik, G., Jensen, M. M., Van De Vossenberg, J., Schmid, M., Woebken, D., et al. (2009). Revising the nitrogen cycle in the Peruvian oxygen minimum zone. *Proceedings of the National Academy of Sciences*, *106*(12), 4752–4757. https://doi.org/10.1073/pnas.0812444106

Levin, L., Gutiérrez, D., Rathburn, A., Neira, C., Sellanes, J., Muñoz, P., et al. (2002). Benthic processes on the Peru margin: A transect across the oxygen minimum zone during the 1997-98 El Niño. *Progress in Oceanography*, *53*, 1–27. https://doi.org/10.1016/s0079-6611(02)00022-8

Lu, Z., Jenkyns, H. C., & Rickaby, R. E. M. (2010). Iodine to calcium ratios in marine carbonate as a paleo-redox proxy during oceanic anoxic events. *Geology*, *38*(12), 1107–1110. https://doi.org/10.1130/g31145.1

Lu, Z., Tomaru, H., & Fehn, U. (2008). Iodine ages of pore waters at Hydrate Ridge (ODP Leg 204), Cascadia Margin: Implications for sources of methane in gas hydrates. *Earth and Planetary Science Letters*, *267*(3–4), 654–665. https://doi.org/10.1016/j.epsl.2007.12.015

Lüdke, J., Dengler, M., Sommer, S., Clemens, D., Thomsen, S., Krahmann, G., et al. (2020). Influence of intraseasonal eastern boundary circulation variability on hydrography and biogeochemistry off Peru. *Ocean Science*, *16*(6), 1347–1366. https://doi.org/10.5194/os-16-1347-2020

Luther, III, G. W. (2023). Review on the physical chemistry of iodine transformations in the oceans. *Frontiers in Marine Science*, *10*. https://doi.org/10.3389/fmars.2023.1085618

Mackin, J. E., Aller, R. C., & Ullman, W. J. (1988). The effects of iron reduction and nonsteady-state diagenesis on iodine, ammonium, and boron distributions in sediments from the Amazon continental shelf. *Continental Shelf Research*, *8*(4), 363–386. https://doi.org/10.1016/0278-4343(88)90009-x

Martin, J. B., Gieskes, J. M., Torres, M., & Kastner, M. (1993). Bromine and iodine in Peru margin sediments and pore fluids: Implications for fluid origins. *Geochimica et Cosmochimica Acta*, *57*(18), 4377–4389. https://doi.org/10.1016/0016-7037(93)90489-j

Martinez-Ruiz, F., Kastner, M., Paytan, A., Ortega-Huertas, M., & Bernasconi, S. M. (2000). Geochemical evidence for enhanced productivity during S1 sapropel deposition in the eastern Mediterranean. *Paleoceanography*, *15*(2), 200–209. https://doi.org/10.1029/1999pa000419

Mckay, J. L., Pedersen, T. F., & Mucci, A. (2007). Sedimentary redox conditions in continental margin sediments (N.E. Pacific)—Influence on the accumulation of redox-sensitive trace metals. *Chemical Geology*, *238*(3–4), 180–196. https://doi.org/10.1016/j.chemgeo.2006.11.008

Middelburg, J. J., & Levin, L. A. (2009). Coastal hypoxia and sediment biogeochemistry. *Biogeosciences*, *6*(7), 1273–1293. https://doi.org/10.5194/bg-6-1273-2009

Mohrholz, V., Bartholomae, C., Van Der Plas, A., & Lass, H. (2008). The seasonal variability of the northern Benguela undercurrent and its relation to the oxygen budget on the shelf. *Continental Shelf Research*, *28*(3), 424–441. https://doi.org/10.1016/j.csr.2007.10.001

Moriyasu, R., Bolster, K. M., Hardisty, D. S., Kadko, D. C., Stephens, M. P., & Moffett, J. W. (2023). Meridional survey of the central Pacific reveals iodide accumulation in equatorial surface waters and benthic sources in the abyssal plain. *Global Biogeochemical Cycles*, *37*(3), e2021GB007300. https://doi.org/10.1029/2021gb007300

Moriyasu, R., Evans, N., Bolster, K. M., Hardisty, D. S., & Moffett, J. W. (2020). The distribution and redox speciation of iodine in the Eastern Tropical North Pacific Ocean. *Global Biogeochemical Cycles*, *34*(2), e2019GB006302. https://doi.org/10.1029/2019gb006302

Noffke, A., Hensen, C., Sommer, S., Scholz, F., Bohlen, L., Mosch, T., et al. (2012). Benthic iron and phosphorus fluxes across the Peruvian oxygen minimum zone. *Limnology and Oceanography*, *57*(3), 851–867. https://doi.org/10.4319/lo.2012.57.3.0851

Pedersen, T., & Price, N. (1980). The geochemistry of iodine and bromine in sediments of the Panama Basin. *Journal of Marine Research*, *38*, 397–411.

Pedersen, T. F., Pickering, M., Vogel, J. S., Southon, J. N., & Nelson, D. E. (1988). The response of benthic foraminifera to productivity cycles in the eastern equatorial Pacific: Faunal and geochemical constraints on glacial bottom water oxygen levels. *Paleoceanography*, *3*(2), 157–168. https://doi.org/10.1029/pa003i002p00157

Pennington, J. T., Mahoney, K. L., Kuwahara, V. S., Kolber, D. D., Calienes, R., & Chavez, F. P. (2006). Primary production in the eastern tropical Pacific: A review. *Progress in Oceanography*, *69*(2–4), 285–317. https://doi.org/10.1016/j.pocean.2006.03.012

Plass, A., Schlosser, C., Sommer, S., Dale, A. W., Achterberg, E. P., & Scholz, F. (2020). The control of hydrogen sulfide on benthic iron and cadmium fluxes in the oxygen minimum zone off Peru. *Biogeosciences*, *17*(13), 3685–3704. https://doi.org/10.5194/bg-17-3685-2020

Podder, J., Lin, J., Sun, W., Botis, S. M., Tse, J., Chen, N., et al. (2017). Iodate in calcite and vaterite: Insights from synchrotron X-ray absorption spectroscopy and first-principles calculations. *Geochimica et Cosmochimica Acta*, *198*, 218–228. https://doi.org/10.1016/j.gca.2016.11.032

Price, N. B., & Calvert, S. E. (1973). The geochemistry of iodine in oxidised and reduced recent marine sediments. *Geochimica et Cosmochimica Acta*, *37*(9), 2149–2158. https://doi.org/10.1016/0016-7037(73)90013-6

Price, N. B., & Calvert, S. E. (1977). The contrasting geochemical behaviours of iodine and bromine in recent sediments from the Namibian shelf. *Geochimica et Cosmochimica Acta*, *41*(12), 1769–1775. https://doi.org/10.1016/0016-7037(77)90209-5

Rapp, I., Schlosser, C., Browning, T. J., Wolf, F., Le Moigne, F. A. C., Gledhill, M., & Achterberg, E. P. (2020). El Niño-driven oxygenation impacts Peruvian shelf iron supply to the South Pacific Ocean. *Geophysical Research Letters*, *47*(7), e2019GL086631. https://doi.org/10.1029/2019gl086631

Redfield, A. C. (1958). The biological control of chemical factors in the environment. *American Scientist*, *46*, 205–221.

Romarís-Hortas, V., Moreda-Piñeiro, A., & Bermejo-Barrera, P. (2009). Microwave assisted extraction of iodine and bromine from edible seaweed for inductively coupled plasma-mass spectrometry determination. *Talanta*, *79*(3), 947–952. https://doi.org/10.1016/j.talanta.2009.05.036

Rue, E. L., Smith, G. J., Cutter, G. A., & Bruland, K. W. (1997). The response of trace element redox couples to suboxic conditions in the water column. *Deep Sea Research Part I: Oceanographic Research Papers*, *44*(1), 113–134. https://doi.org/10.1016/s0967-0637(96)00088-x

Schlosser, C., Streu, P., Frank, M., Lavik, G., Croot, P. L., Dengler, M., & Achterberg, E. P. (2018). H2S events in the Peruvian oxygen minimum zone facilitate enhanced dissolved Fe concentrations. *Scientific Reports*, *8*, 1–8. https://doi.org/10.1038/s41598-018-30580-w

Scholz, F. (2018). Identifying oxygen minimum zone-type biogeochemical cycling in Earth history using inorganic geochemical proxies. *Earth-Science Reviews*, *184*, 29–45. https://doi.org/10.1016/j.earscirev.2018.08.002

Scholz, F., & Hardisty, D. (2023). Solid phase iodine data for sediment cores from METEOR cruises M136 and M137 [Dataset]. PANGAEA. https://doi.org/10.1594/PANGAEA.963218

Scholz, F., Hensen, C., Lu, Z., & Fehn, U. (2010). Controls on the 129I/I ratio of deep-seated marine interstitial fluids: 'Old' organic versus fissiogenic 129-iodine. *Earth and Planetary Science Letters*, *294*(1–2), 27–36. https://doi.org/10.1016/j.epsl.2010.02.034

Scholz, F., Hensen, C., Noffke, A., Rohde, A., Liebetrau, V., & Wallmann, K. (2011). Early diagenesis of redox-sensitive trace metals in the Peru upwelling area: Response to ENSO-related oxygen fluctuations in the water column. *Geochimica et Cosmochimica Acta*, *75*(22), 7257–7276. https://doi.org/10.1016/j.gca.2011.08.007

Scholz, F., Löscher, C. R., Fiskal, A., Sommer, S., Hensen, C., Lomnitz, U., et al. (2016). Nitrate-dependent iron oxidation limits iron transport in anoxic ocean regions. *Earth and Planetary Science Letters*, *454*, 272–281. https://doi.org/10.1016/j.epsl.2016.09.025

Scripps Institution of Oceanography. (1978). *Physical and chemical data, CIRCE expedition, 16 March-1 December 1968*. University of California, Scripps Institution of Oceanography.

Sellner, K. G., Hendrikson, P., & Ochoa, N. (1983). Relationships between the chemical composition of particulate organic matter and phytoplankton distributions in recently upwelled waters off Peru. *Coastal Upwelling Its Sediment Record: Part A: Responses of the Sedimentary Regime to Present Coastal Upwelling* (pp. 273–287).

Shaikh, A., Kurian, S., Shenoy, D. M., Pratihary, A. K., Dais, A. B., Naik, R., & Borker, S. G. (2023). Spatial and temporal variation of dissolved iodine in the eastern Arabian Sea. *Marine Chemistry*, *257*, 104322. https://doi.org/10.1016/j.marchem.2023.104322

Sommer, S., & Dale, A. W. (2021). Benthic work during METEOR cruise M136 [Dataset]. PANGAEA. https://doi.org/10.1594/PANGAEA.928280

Stramma, L., Fischer, T., Grundle, D. S., Krahmann, G., Bange, H. W., & Marandino, C. A. (2016). Observed El Niño conditions in the eastern tropical Pacific in October 2015. *Ocean Sciences*, *12*(4), 861–873. https://doi.org/10.5194/os-12-861-2016

Thamdrup, B., Dalsgaard, T., & Revsbech, N. P. (2012). Widespread functional anoxia in the oxygen minimum zone of the Eastern South Pacific. *Deep Sea Research Part I: Oceanographic Research Papers*, *65*, 36–45. https://doi.org/10.1016/j.dsr.2012.03.001

Truesdale, V. W., & Luther, III, G. W. (1995). Molecular iodine reduction by natural and model organic substances in seawater. *Aquatic Geochemistry*, *1*, 89–104. https://doi.org/10.1007/bf01025232

Tsunogai, S. (1971). Iodine in the deep water of the ocean. *Deep-Sea Research*, *18*(9), 913–919. https://doi.org/10.1016/0011-7471(71)90065-9

Ullman, W. J., & Aller, R. C. (1980). Dissolved iodine flux from estuarine sediments and implications for the enrichment of iodine at the sediment water interface. *Geochimica et Cosmochimica Acta*, *44*(8), 1177–1184. https://doi.org/10.1016/0016-7037(80)90071-x

Ullman, W. J., & Aller, R. C. (1983). Rates of iodine remineralization in terrigenous near-shore sediments. *Geochimica et Cosmochimica Acta*, *47*(8), 1423–1432. https://doi.org/10.1016/0016-7037(83)90301-0

Ullman, W. J., & Aller, R. C. (1985). The geochemistry of iodine in near-shore carbonate sediments. *Geochimica et Cosmochimica Acta*, *49*(4), 967–978. https://doi.org/10.1016/0016-7037(85)90311-4

Upstill-Goddard, R. C., & Elderfield, H. (1988). The role of diagenesis in the estuarine budgets of iodine and bromine. *Continental Shelf Research*, *8*(4), 405–430. https://doi.org/10.1016/0278-4343(88)90012-x

Vedamati, J., Goepfert, T., & Moffett, J. W. (2014). Iron speciation in the eastern tropical South Pacific oxygen minimum zone off Peru. *Limnology and Oceanography*, *59*(6), 1945–1957. https://doi.org/10.4319/lo.2014.59.6.1945

Veeh, H. H., Calvert, S. E., & Price, N. B. (1974). Accumulation of uranium in sediments and phosphorites on the South West African shelf. *Marine Chemistry*, *2*(3), 189–202.

Wong, G. T. F. (1977). The distribution of iodine in the upper layers of the equatorial Atlantic. *Deep-Sea Research*, *24*(2), 115–125. https://doi.org/10.1016/0146-6291(77)90547-1

Wong, G. T. F., & Brewer, P. G. (1974). The determination and distribution of iodate in South Atlantic waters. *Journal of Marine Research*, *32*, 25–36.

Wong, G. T. F., & Brewer, P. G. (1977). The marine chemistry of iodine in anoxic basins. *Geochimica et Cosmochimica Acta*, *41*(1), 151–159. https://doi.org/10.1016/0016-7037(77)90195-8

Zhou, X., Jenkyns, H. C., Lu, W., Hardisty, D. S., Owens, J. D., Lyons, T. W., & Lu, Z. (2017). Organically bound iodine as a bottom-water redox proxy: Preliminary validation and application. *Chemical Geology*, *457*, 95–106. https://doi.org/10.1016/j.chemgeo.2017.03.016

References From the Supporting Information

Boudreau, B. P. (1997). *Diagenetic models and their implementation* (p. 414). Springer Verlag.

Dale, A. W., Paul, K. M., Clemens, D., Scholz, F., Schroller-Lomnitz, U., Wallmann, K., et al. (2021). Recycling and burial of biogenic silica in an open margin oxygen minimum zone. *Global Biogeochemical Cycles*, *35*(2), e2020GB006583. https://doi.org/10.1029/2020gb006583